A Comparison of Modeled and Observed Relationships between Interannual Variations of Water Vapor and Temperature

DE-ZHENG SUN

Program in Atmospheric and Oceanic Sciences, Princeton University, Princeton, New Jersey

ISAAC M. HELD

Geophysical Fluid Dynamics Laboratory/NOAA, Princeton, New Jersey

(Manuscript received 3 April 1995, in final form 9 August 1995)

ABSTRACT

The correlations between interannual variations of tropical mean water vapor and temperature in the simulations by a low resolution (R15) GCM are stronger than those in the rawinsonde observations. The rate of fractional increase of tropical mean water vapor with temperature in the model simulations is also larger than that from the observations. The largest discrepancies are found in the region immediately above the tropical convective boundary layer (850–600 mb). The rate of fractional increase of tropical mean water vapor with temperature in the model simulations is close to that for a constant relative humidity. The correlations between variations of water vapor in the upper troposphere and those in the lower troposphere are also stronger in the model simulations than in the observations. In the horizontal, the characteristic spatial patterns of the normalized water vapor variations in the model simulations and observations are similar. The water vapor–temperature relationship in simulations by a GCM with a somewhat higher spatial resolution (R30) is almost identical to that in the simulations by the low resolution (R15) GCM. The implications of these findings for the radiative feedback of water vapor are discussed.

1. Introduction

Central to the stability and sensitivity of the climate system is the relationship between water vapor and temperature. Manabe and Wetherald (1967) demonstrated that a radiative–convective model with fixed relative humidity is roughly twice as sensitive to CO_2 increases as is a model with fixed specific humidity. GCM simulations have generally supported this estimate of the strength of the water vapor feedback and the relevance of the fixed relative humidity assumption (Cess et al. 1990; IPCC 1992). The strength of this feedback has recently been questioned (Lindzen 1990; Sun and Lindzen 1993a,b), based on a critique of the realism of the mechanisms that maintain the humidity distribution in GCMs. In particular, Sun and Lindzen (1993a,b) raised the importance of the evaporation of hydrometeors and the need to examine the water vapor–temperature relationship as a function of height.

The mean temperature of the tropical atmosphere (temperature horizontally averaged over the tropical domain) possesses significant interannual variability,

mostly related to the ENSO (El Niño and Southern Oscillation) phenomenon. As recently documented by Sun and Oort (1995), there are changes in the tropical mean water vapor that are correlated with these temperature changes. One can test a GCM's maintenance of the relative humidity by seeing whether it can simulate this observed relationship when observed variations in sea surface temperature are imposed. In this paper we examine these variations in a low resolution (R15) GCM that has been used extensively for global warming studies at GFDL, and more briefly, in a somewhat higher-resolution (R30) model.

Our focus is on the horizontal averages over the entire Tropics rather than more local structures. When convection is redistributed in an ENSO event, water vapor is redistributed with a very similar pattern, as seen in radiosonde data (Sun and Oort 1995) and in satellite-derived upper-tropospheric water vapor (Soden and Fu 1995). However, in addition to this redistribution, there is evidently also an increase in the tropical mean water vapor. We are interested in how the mean water vapor of the tropical atmosphere adjusts to the change in the mean tropical temperature. In response to an increase of CO_2, one also expects an increase in the mean temperature of the tropical atmosphere. Though it is not clear whether the relationship between the tropical mean water vapor and temperature

―――――――――――
Corresponding author address: Dr. De-Zheng Sun, NCAR, P.O. Box 3000, Boulder, CO 80307-3000.
E-mail: dns@ncar.ucar.edu

on the interannual timescale is the same as that in global warming, the ability of a GCM to simulate this relationship is an important test of the relevant model physics. The hope is that the relationship between the tropical mean water vapor and temperature is mostly a function of the vertical transport to which moist convection is the primary contributor, rather than the horizontal transport by the large-scale circulation.

We first describe the data and methods used for our analysis in section 2. In section 3, we compare the relationship between variations of tropical mean water vapor and temperature in the R15 GCM with those in the rawinsonde observations. In section 4, we compare the spatial structure of water vapor variations in the R15 model with those in the rawinsonde observations. In section 5, we briefly examine the water vapor–temperature relationship in the R30 model. We summarize our findings and discuss their implications in section 6.

2. Data and methods

The GCM simulations that we compare with rawinsonde observations are from experiments conducted at GFDL described by Lau and Nath (1994). The GCM has 9 sigma levels in the vertical and a rhomboidal spectral truncation at wavenumber 15. Moist convection in the model is parameterized by the convective-adjustment scheme (Manabe et al. 1965). The model has realistic orography and land–sea contrast. Between 40°S and 60°N, observed monthly varying sea surface temperature (SST) was used as the lower boundary condition for the model simulations. In the oceanic region outside 40°S–60°N, climatological SST was used as the lower boundary condition. The experiment was performed for a 43-yr period from January 1946 through December 1988. We are interested only in the period from May 1963 through December 1988 for which analyzed global rawinsonde records are available (Oort 1983, updated). Four parallel GCM integrations starting from different initial conditions are available (for more details, see Lau and Nath 1994). In most calculations presented in this article, there are no significant differences between the results obtained using the data from a single experiment and those from the ensemble average. Unless explicitly mentioned, all results presented in this article are obtained using monthly mean data from a single experiment. The original model data on sigma levels were interpolated to 9 pressure levels (990, 940, 830, 680, 515, 350, 205, 95, and 25 mb) close to the sigma levels prespecified in the model. Rawinsonde data for water vapor are available on the traditional mandatory levels up to the 300-mb level (Oort 1983). When a comparison needs to be made on the same level, we further interpolate the model data at the nine pressure levels to the mandatory levels.

In addition to the simulations by the R15 model, we also have simulations by a somewhat higher-resolution model (R30) for a more limited period (January 1979 through December 1988). The R30 model has five more levels than the R15 model (four more levels in the tropical troposphere). Other aspects of the R30 model are very similar to the R15 model.

As in Sun and Oort (1995), we decompose the variations of temperature and specific humidity into three parts:

$$T = T_s + T_a + T_l \tag{1}$$

$$q = q_s + q_a + q_l. \tag{2}$$

The subscripts s, a, and l represent, respectively, the normal seasonal cycle, interannual variability, and the long-term trend. In deriving the relationship between water vapor and temperature, it is desirable to separate the signals that correspond to different physical causes. The physical causes for the long-term trends in the observational data are obscure, and there is concern that the long-term trend in the humidity data may be due to systematic errors that are related to changes of instrument (Elliott and Gaffen 1991; Gaffen et al. 1991; Sun and Oort 1995). We want to extract the relationship between water vapor and temperature from variations of T_a and q_a through correlation and regression analyses. To obtain T_a and q_a from T and q for the period May 1963–December 1988, we take T_l and q_l as the linear trend of the time series of T and q over that period, and T_s and q_s as the mean seasonal cycle over the period 1964–1973. Using the 1964–73 climatology instead of the climatology for the whole period is consistent with the historical way radiosonde data at GFDL have been analyzed and gridded (Oort 1983). When the simulations by the R15 model are further compared with those by the R30 model over the period 1979–1988, we obtain T_a and q_a from T and q by taking T_s and q_s as the mean seasonal cycle over the period 1979–1988, and T_l and q_l as the linear trend of T and q over the period 1979–1988.

In the following text, we will use $\langle q_a \rangle$ and $\langle T_a \rangle$ to represent the tropical mean values (30°S–30°N) for q_a and T_a. The tropical mean values for the annually averaged T_s and q_s will be represented by $\langle \bar{T} \rangle$ and $\langle \bar{q} \rangle$. The functional dependence of tropical mean water vapor on temperature will be quantified by the rate of fractional increase of water vapor with temperature $[\gamma = (1/q)(dq/dT)]$. Comparing the effects of water vapor at different levels in the atmosphere, Shine and Sinha (1991) have found that the radiative feedback of water vapor in greenhouse warming is approximately proportional to the fractional increase of water vapor. We estimate γ by using a linear regression:

$$\frac{\langle q_a \rangle}{\langle \bar{q} \rangle} = \alpha + \gamma \langle T_a \rangle. \tag{3}$$

The variations of T_a are small enough that this linear approximation should be adequate (Sun and Oort 1995). Linear correlation maps and empirical orthog-

onal functions (EOFs) will be used to examine the spatial structure of water vapor variations.

3. Relationship between variations of tropical mean water vapor and temperature

a. Correlation and regression analysis

In both the model simulations and observations, $\langle T_a \rangle$ and $\langle q_a \rangle$ have significant vertically coherent variations. The simulated $\langle T_a \rangle$ agrees very well with those of the observed $\langle T_a \rangle$ in both the upper and lower troposphere, while there are significant discrepancies between the simulated and observed $\langle q_a \rangle$ above the tropical convective boundary layer. Figure 1 presents the variations of $\langle T_a \rangle$ (a) and $\langle q_a \rangle / \langle \bar{q} \rangle$ (b) at two representative levels (500 and 850 mb). The solid lines are for the simulated variations, while the dashed lines are the observations. Peak positive anomalies of $\langle T_a \rangle$ correspond with important El Niño events. The magnitude of $\langle T_a \rangle$ increases with height (from about 0.5 K in the surface boundary layer to about 1 K in the upper troposphere). Relative to the mean specific humidity ($\langle \bar{q} \rangle$), the magnitude of $\langle q_a \rangle$ also increases with height (from about 5% in the surface boundary layer to about 10% in the upper troposphere). The vertical profile of $\langle \bar{q} \rangle$ is shown in Fig. 2a. Away from the surface, $\langle \bar{q} \rangle$ from the model simulations is significantly smaller than $\langle \bar{q} \rangle$ from the observations. This difference is primarily due to a cold bias in the model-simulated mean temperature. Figure 2b shows the vertical profile of the relative humidity for the tropical mean atmosphere ($\langle \bar{q} \rangle$ divided by the saturation specific humidity for the mean tropical atmosphere). In terms of relative humidity, the model atmosphere is slightly moister than the observed atmosphere.

In both the observations and the model simulations, the variations of $\langle q_a \rangle$ are positively correlated with the variations of $\langle T_a \rangle$. Figure 3 presents the time series of $\langle q_a \rangle$ normalized by its standard derivation (solid line), superposed on the time series of normalized T_a (dashed line). Figure 3 shows that the correlations between $\langle q_a \rangle$ and $\langle T_a \rangle$ are much greater in the model simulations than in the observations. A high noise level in the observed $\langle q_a \rangle$, perhaps due to sampling error, may contribute significantly to this discrepancy. More interesting are the differences in the vertical structure of the correlation coefficients between $\langle q_a \rangle$ and $\langle T_a \rangle$ as shown in Fig. 4. Monthly mean data were used for the calculations. The correlation coefficients between the observed $\langle T_a \rangle$ and $\langle q_a \rangle$ decrease quickly away from the surface to a minimum value at 700 mb, while the correlation coefficients between the simulated $\langle T_a \rangle$ and $\langle q_a \rangle$ remain approximately constant with height.

Figure 5 presents the rate of fractional increase of water vapor with temperature γ as obtained from (3) and least-squares linear regression. If there are sampling or instrumental errors in the observed $\langle q_a \rangle$, they
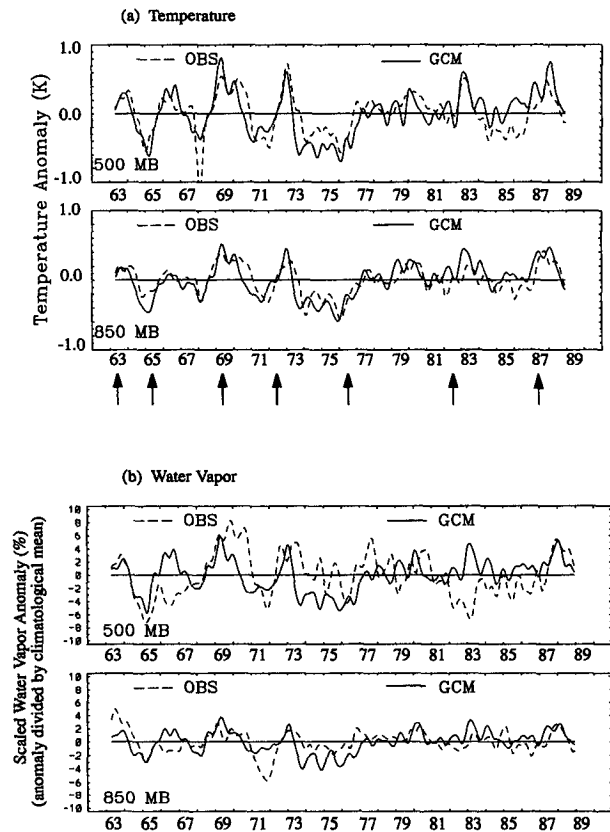

FIG. 1. (a) Time series for model simulated (solid line) and observed (dashed line) $\langle T_a \rangle$. Monthly mean data were smoothed by using a cosine bell window (the Hanning window) with a width of 7 months. The coefficients of this window are given by $h_n = H_n / \Sigma_1^N H_n$ with $H_n = 0.5 \{1 - \cos[2\pi(n)/N + 1]\}$, where $n = 1, 2, \ldots N$ and N is the width of the window. Important El Niño events are indicated by arrows at the bottom of the figure. (b) Time series for model simulated (solid line) and observed (dashed line) $\langle q_a \rangle / \langle \bar{q} \rangle$. Monthly mean data were smoothed by using the Hanning window with a width of 7 months.

will not affect γ if they are uncorrelated with $\langle T_a \rangle$. For comparison, the rate of fractional increase of water vapor with temperature for constant relative humidity [$\gamma^* = (1/q^*)/dq^*/dT$] with q^* being the saturation specific humidity] is also presented in Fig. 5. The tropical mean temperature $\langle \bar{T} \rangle$ and the saturation water vapor pressure over pure liquid water were used to calculate γ^*. We see from Fig. 5 that in the region approximately between 850 and 500 mb, the rate of fractional increase of water vapor with temperature from the observations is considerably smaller than that from the model simulations. The largest discrepancies between the two rates occur in the region immediately above the tropical convective boundary layer. Except in the region near the surface (below 850 mb), the rate of fractional increase of water vapor with temperature from the model simulations is very close to that for a constant relative humidity. Thus, in the GCM the water vapor–temper-

ature relationship on the interannual timescale is similar to that in global warming simulations in several models (Cess et al. 1990; IPCC 1992).

b. Estimates of greenhouse effect

The stronger dependence of water vapor on temperature in the model simulations implies a stronger radiative feedback of water vapor. Figure 6 shows the relationships between the outgoing longwave radiation at the top of the atmosphere (F) and surface temperature (T_s) that correspond to three different assumptions about the relationship between water vapor and temperature. Blackbody radiation curves at temperatures T_s $- 26$ and $T_s - 32$ are also presented for reference (thick solid lines). The solid line in Fig. 6 was obtained using the γ from the model except in the region above 100 mb where we have assumed that the relative humidity (h) is fixed. The data in the model stratosphere are considered unreliable. The short-dashed line was obtained using the γ for the observed atmosphere. Since there are no observational data above 300 mb, we have assumed that h is fixed in that region. The long-dashed line corresponds to a fixed relative humidity. The reference relative humidity distribution is the same as used by Manabe and Wetherald (1967). The lapse rate is fixed to the climatological values for the tropical atmosphere given by McClatchey et al. (1972). The sea–air temperature difference is fixed at 1 K. The radiation code is that of Chou (1986) and Chou et al. (1991), and includes water vapor, CO_2, O_3, CH_4, and N_2O. No aerosols or clouds are included. The vertical resolution used for our calculations is the same as in Sun and Lindzen (1993b). Taking the reference surface temperature as 300 K, we find $dF/dT_s = 2.4$ W m^{-2} K^{-1} for an atmosphere with constant relative humidity, $dF/dT_s = 2.5$ W m^{-2} K^{-1} for the GCM, and $dF/dT_s = 3.2$ W m^{-2} K^{-1} for the observed atmosphere. Note that for blackbody radiation, dF/dT_s is about 6.2 W m^{-2} K^{-1}. These estimates are for the Tropics only and for clear sky. If one assumes fixed relative humidity in the extratropics, the difference between the observed value and that for fixed relative humidity, averaged over the globe, would be reduced by a factor of two. If one accepts the hypothesis that the tropical mean water vapor–temperature relationship obtained from interannual variability is relevant for the Tropics in global warming studies, the global warming would be reduced by about 15% from that predicted in the GCM. This is significant, but it is a relatively small source of uncertainty compared to the uncertainties in cloud feedback (Cess et al. 1989). It should be cautioned, however, that this estimate is based on a one-dimensional model, and thus it involves the assumption that the increase of water vapor in the Tropics in response to global warming is horizontally homogeneous. The characteristic changes of water vapor associated with ENSO events are not horizontally homogeneous. Increases of water
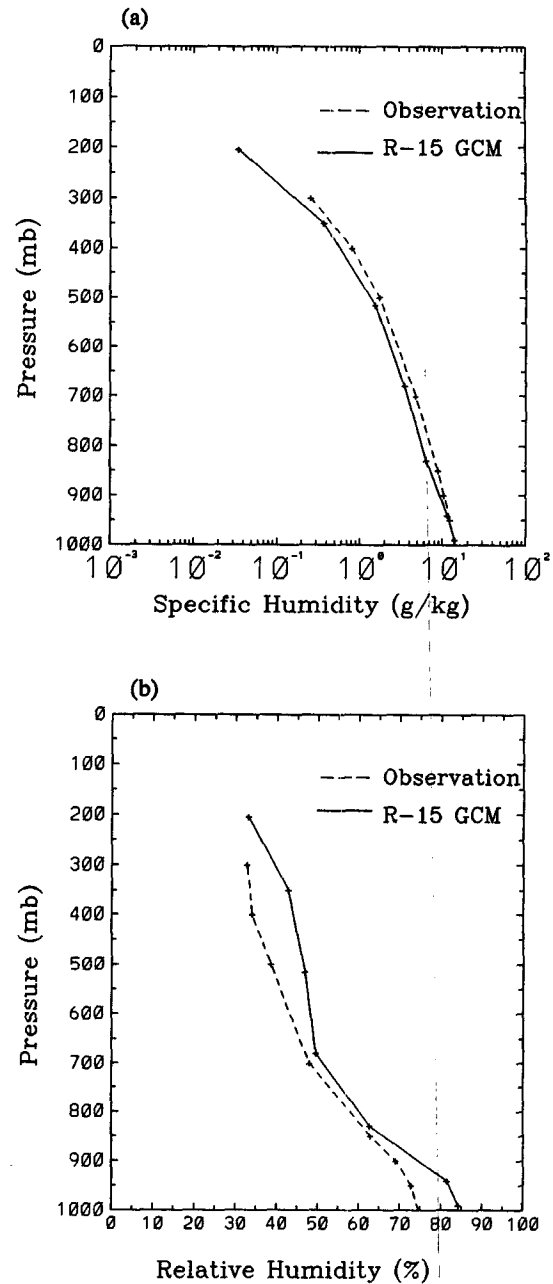

(a)

(b)

FIG. 2. (a) Vertical profile of $\langle \bar{q} \rangle$ for the model (solid line) and the observed atmosphere (dashed line). (b) Vertical profile of $\langle \bar{q} \rangle/q^*(\langle \bar{T} \rangle)$ for the model (solid line) and the observed atmosphere (dashed line). Saturation water vapor pressure over pure liquid water was used to calculate $q^*(\langle \bar{T} \rangle)$. Here $\langle \bar{q} \rangle$ and $\langle \bar{T} \rangle$ are from the 1964–1973 climatology.

vapor in the eastern Pacific are actually accompanied with decreases of water vapor in the western Pacific (Sun and Oort 1995; Soden and Fu 1995). However, such a pattern of change is associated with the redistribution of moist convection, which probably will not occur during global warming.

(a) GCM
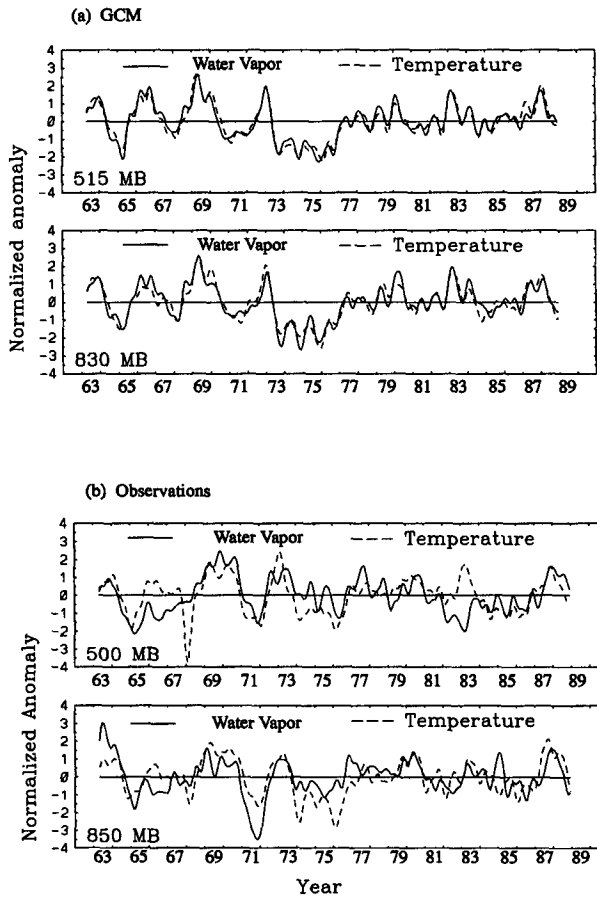

(b) Observations

FIG. 3. Time series for normalized $\langle T_a \rangle$ and $\langle q_a \rangle$ from the model simulations (a) and observations (b). Data were smoothed by using the Hanning window with a width of 7 months.
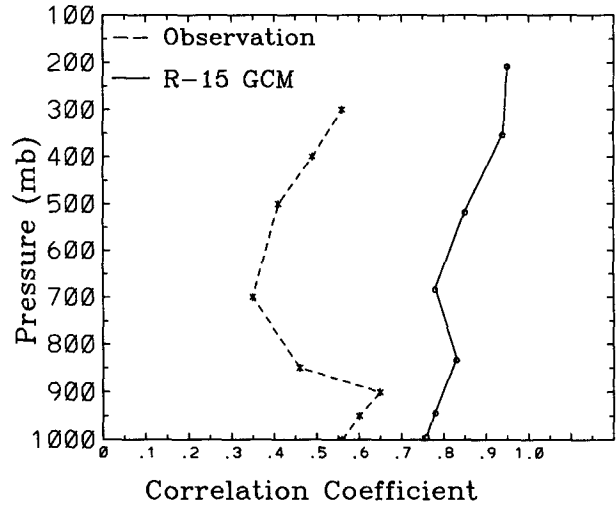

FIG. 4. Vertical structure of correlations between variations of $\langle T_a \rangle$ and $\langle q_a \rangle$ from the model simulations (solid line) and observations (dashed line). The pressure levels for which the calculations were made are marked by "+" for the observations and "O" for the model simulations.

western tropical Pacific region is defined here as the tropical belt between 105°E and the date line. The solid lines are the model simulation, while the dashed lines are the observations. Apparently, there are also significant differences between the model-simulated variations and the observations over the western tropical Pacific region. Figure 7b further shows the differences between the γ from the model simulations and that from the observations over the western Pacific region.

c. Potential problems in rawinsonde data

To correctly interpret the differences between the water vapor–temperature relationship from the model simulations and that from the observations shown in Fig. 5, one also has to consider two major potential problems in the rawinsonde observations. One is the relatively poor spatial coverage of the rawinsonde network over the eastern tropical Pacific Ocean, which may introduce some errors in the estimate of the tropical mean water vapor (Sun and Oort 1995). The other problem is related to changes of instruments during the course of the record, which may have introduced erroneous variations of water vapor.

We have not attempted a thorough analysis of possible errors due to spatial sampling, but we do not believe that these can account for most of the model-observation differences, since we see similar differences when averaging only over relatively data-rich regions, such as the western Pacific. Figure 7a shows the variations of the area-averaged water vapor over the western Pacific region at 500 and 850 mb. The
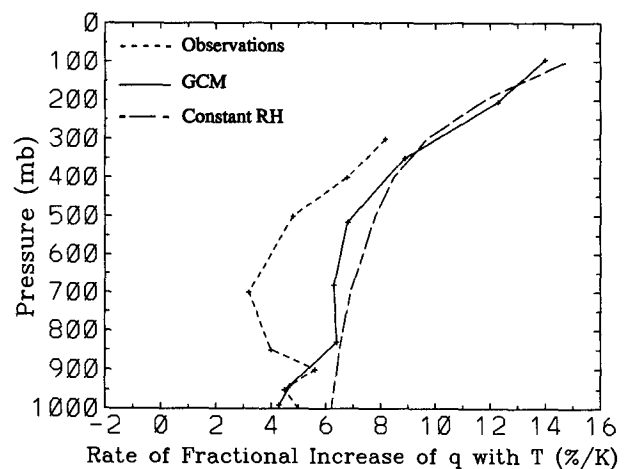

FIG. 5. Vertical structure of the rate of fractional increase of tropical mean water vapor with temperature for the model (solid line), the observed atmosphere (short-dashed line) and a constant relative humidity (long-dashed line). The pressure levels for which the calculations were made are marked by "+" (see text for more information).
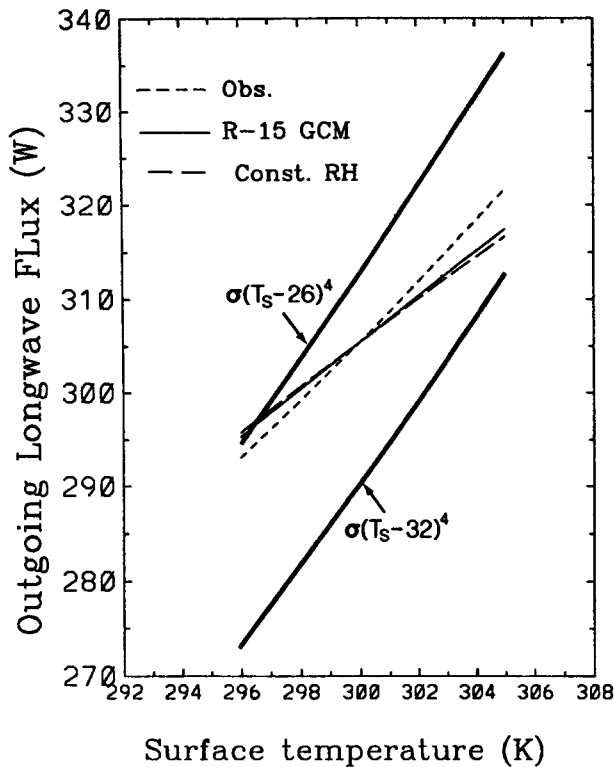
FIG. 6. The rate of increase of the net outgoing radiation at the top of the atmosphere with surface temperature for the model (solid line), the observed atmosphere (short-dashed line), and an atmosphere with a fixed relative humidity (long-dashed line). The two thick solid lines are blackbody radiation at temperatures $T_s - 32$ and $T_s - 26$ (see text for more details of the calculation).

When we limit the time series for the calculation to the period January 1973 through December 1988, during which there were no major changes of instruments (Gaffen et al. 1991), the differences between the rate of change of water vapor with temperature from the observations and that from the GCM simulations become even larger (Fig. 8). Based on these calculations, we think that it would be prudent to assume that there are inadequacies in the model physics, though it is still possible that part of the data-model discrepancies may also be due to errors in the observational data.

4. Vertical and horizontal structures of water vapor variations

a. Correlations with surface variations

Stronger vertical mixing of water vapor in the model atmosphere could lead to a stronger link between variations of water vapor and temperature than exists in the atmosphere. At the surface level, evaporation of water vapor from the surface leads to a strong link between variations of water vapor and those of temperature. In general, the temperature variations in the interior of the

tropical troposphere are strongly coupled with those at the surface. A stronger vertical mixing of water vapor leads to a stronger coupling between the variations of water vapor in the interior of the troposphere and those at the surface level, and consequently to a stronger coupling with the variations of temperature.

The coupling between the variations of water vapor in the interior of the troposphere and those at the surface is indeed much stronger in the model simulations than in the observations. Figure 9 shows the correlation coefficients between the variation of tropical mean water vapor at all heights of the troposphere with those at the lowest level. (The lowest levels for the observations and the model simulations are 1000 and 990 mb, respectively. In the subsequent text, we will refer to these two levels as the surface level.) While the correlations with the surface variations in the observed atmosphere decrease quickly with height, the correlations with the surface variations in the model atmosphere remain roughly constant with height.
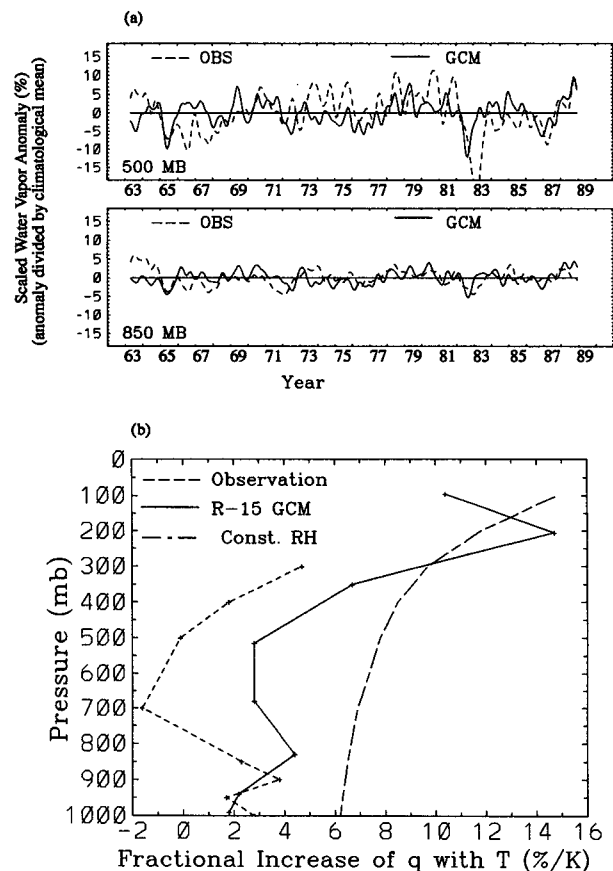

FIG. 7. (a) Time series for q_a averaged over the western Pacific Ocean (the tropical region between 105°E and the date line). (b) Vertical structure of the rate of fractional increase of water vapor averaged over the western Pacific Ocean with tropical mean temperature. Line patterns and symbols have the same meaning as in Fig. 5.
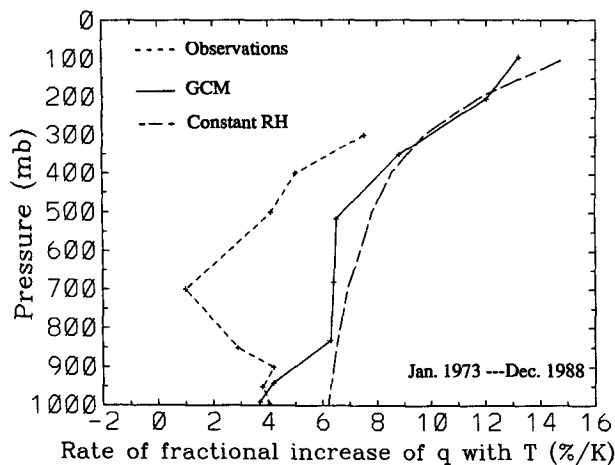
FIG. 8. Vertical structure of the rate of fractional increase of tropical mean water vapor with temperature. In this calculation, data before January 1973 are not included. Line patterns and symbols have the same meaning as in Fig. 5.

To show the connection between the strength of the correlations with the surface variations and the intensity and frequency of deep convection, we further present in Fig. 10 a cross section of correlations between the variations of zonal mean q_a and those at the surface level at the same latitude. The upper figure is for the model atmosphere and the lower figure for the observed
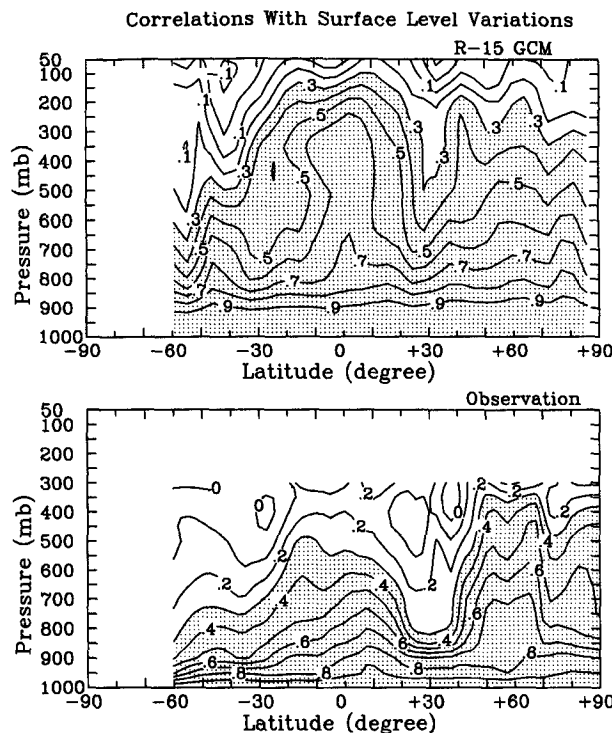

FIG. 10. Cross section of the correlations between variations of zonal mean specific humidity and those at the surface. Upper: model simulations; lower: observations. Areas with a correlation coefficient greater than 0.3 are shaded.
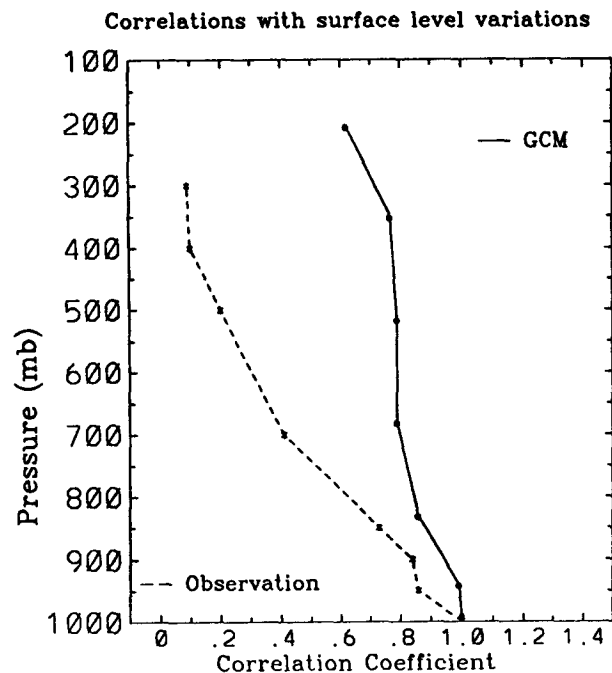
FIG. 9. Correlations between variations of $\langle q_a \rangle$ and those at the lowest level. Symbols "*" and "O" have the same meaning as in Fig. 4.

atmosphere. Figure 10 shows that in both the model and observed atmosphere, the correlations tend to reach maximum values in the deep Tropics and the midlatitude eddy regime. The pattern is consistent with the meridional distribution of latent heat release and precipitation (Peixoto and Oort 1992). However, in the deep Tropics, the correlations between the variations of water vapor and those at the surface level are much stronger in the model than in the observed atmosphere. Note that there are also discrepancies in the surface boundary layer.

Figure 11 presents a cross section of correlations between variations of zonal mean temperature and those at the surface. In the deep Tropics, the agreement in the case of temperature between the model simulations and the observations is much better. Figure 12 further presents a cross section of the correlation coefficients between variations of zonal mean water vapor and the zonal mean temperature at the same height and latitude. In both the observations and the model simulations, the correlations between the variations of water vapor and temperature are stronger in regions where the correlations with the surface variations are stronger.

b. EOF analysis of the horizontal structure

For the same reason that a stronger vertical mixing of water vapor may lead to a stronger link between

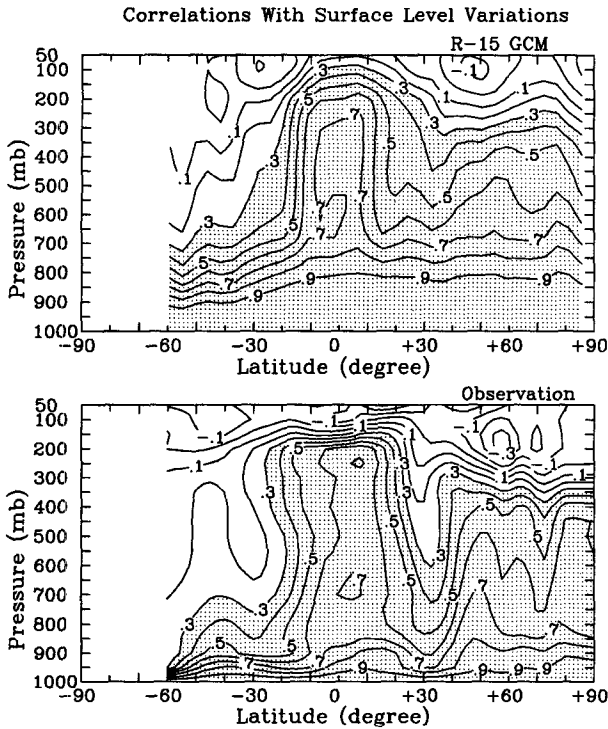Correlations With Surface Level Variations

FIG. 11. Cross section of the correlations between variations of zonal mean temperature and those at the surface. Upper: model simulations; lower: observations. Areas with a correlation coefficient greater than 0.3 are shaded.

variations of water vapor and temperature, a stronger mixing of water vapor between the ascending and descending branches of the Hadley or Walker circulation can also lead to a stronger link between the variations of water vapor and temperature.

The horizontal structure of the normalized variations of water vapor in the model simulations is similar to that in the observations, which suggests that the mixing of water vapor in the horizontal in the GCM simulations may not be very different from that in the observations. Figure 13 shows the leading EOF of the normalized variations of the monthly mean q_a at the 500-mb level. Figures 13a and 13c are from the model simulations and Fig. 13b from the observations. Figure 13a is obtained using variations of water vapor from a single experiment and Fig. 13c from an ensemble average of the four parallel experiments (refer to section 2). There are some differences between Figs. 13a and 13c over the Indian Ocean (which is the main reason we present both of them here). Figures 13a and 13c are indeed quite similar to Fig. 13b, although there are also some noticeable discrepancies. The spatial pattern of the leading EOF corresponds well with the phenomenon of ENSO, with the variations of water vapor in the western Pacific Ocean having the opposite sign to the variations of water vapor in the eastern Pacific

Ocean. The percentage variance that the leading EOF accounts for, however, is small. The leading EOFs in Fig. 13a, 13b, and 13c account for, respectively, 6%, 11%, and 9% of the total variance of water vapor variations at 500 mb. This is partly because monthly mean data were used in this calculation. When a Hanning window with a width of 7 months was used to smooth the data, we find that the spatial pattern of the leading EOF remains the same but that the percentage variance of the leading EOF explains increases significantly (21% for the EOF in Fig. 13a, 17% for the EOF in Fig. 13b, and 22% for the EOF in Fig. 13c).

We further present in Fig. 14 the first EOF of the normalized zonal mean variations of q_a in the tropical region. The upper figure is for the model atmosphere and the lower figure for the observed atmosphere. Note that compared to the pattern of the EOF from the observations, the EOF from the model atmosphere is more diffused in the vertical. Both EOFs account for about one-third of the total variance.

5. Water vapor–temperature relationship in a model with a higher resolution

To investigate the role of model resolution, we have further compared the water vapor–temperature relationship in a R30 model with that in the R15 model based on a 10-yr simulation of the atmosphere (January
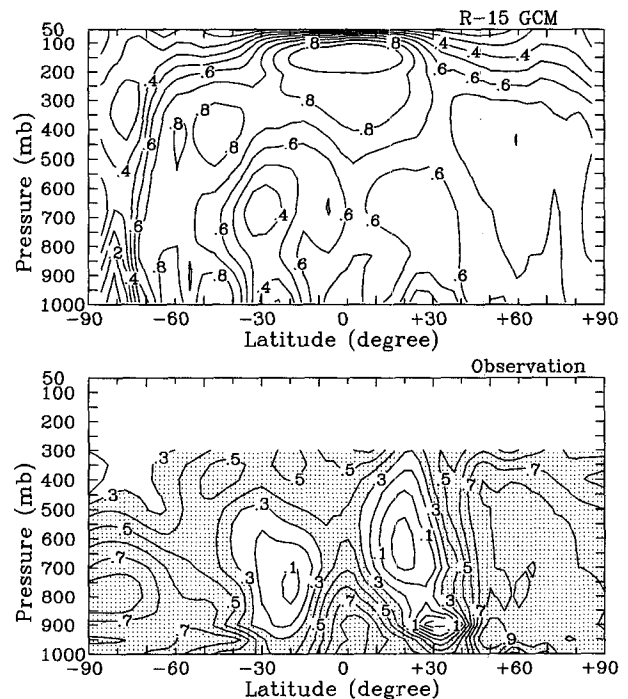

FIG. 12. Cross section of the correlations between variations of zonal mean specific humidity and variations of zonal mean temperature. Upper: model simulations; lower: observations. In the lower panel, areas with correlation coefficient greater than 0.3 are shaded.
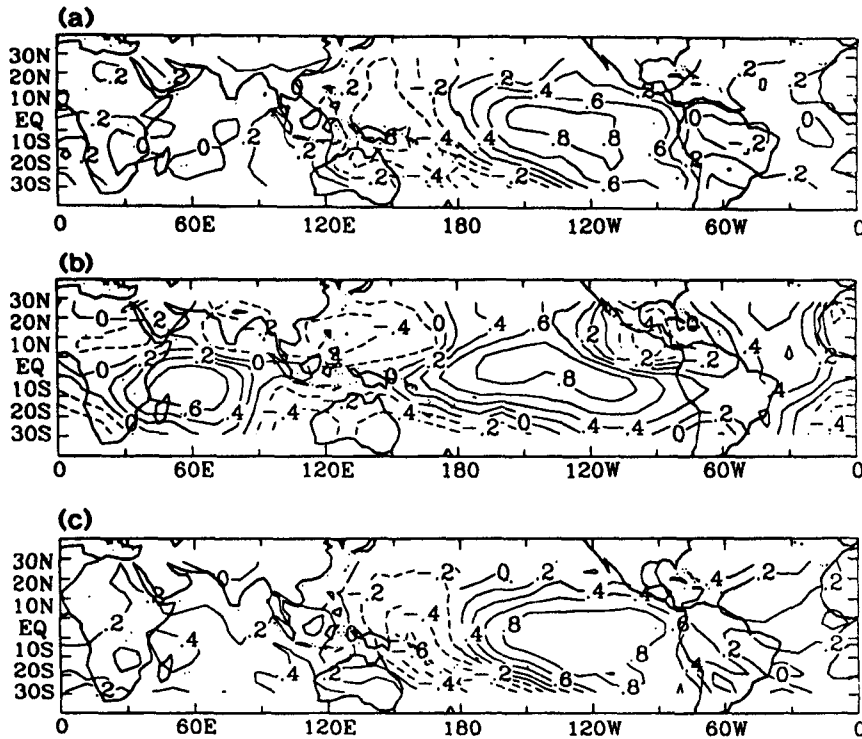
FIG. 13. The first EOF of the normalized variations of q_a at 500 mb. The EOF is normalized so that its maximum value is 1. (a) Here q_a is from a single experiment, (b) q_a is from the observations, and (c) q_a is from the ensemble average of the four parallel experiments (see text for more details).

1979–December 1988). The comparison suggests that the stronger link between the variations of water vapor and temperature is not primarily a problem of insufficient horizontal resolution. Figure 15 shows the vertical structure of the correlation between tropical mean temperature and water vapor, and Fig. 16 shows the vertical structure of the rate of fractional increase of tropical mean water vapor with temperature. We see that the relationship between the variations of the tropical mean water vapor and temperature in the R30 is almost identical to that in the R15. Figure 17 shows cross sections of the correlations between variations of zonal mean water vapor and those at the surface. We see that in the deep Tropics, the correlations between the variations of water vapor in the interior of the troposphere and those at the surface level in the R30 are also as high as those in the R15 model.

6. Summary and discussions

We find that the interannual variations of tropical mean water vapor in the GCM simulations are almost perfectly correlated with the variations of tropical mean temperature. In contrast, the corresponding correlations in the observations are much weaker. The rate of fractional increase of tropical mean water vapor with temperature (γ) in the GCM simulations is also larger than

that in the rawinsonde observations. The largest discrepancies are not found in the upper troposphere, but in the region immediately above the tropical convective boundary layer. The rate of fractional increase of tropical mean water vapor (γ) in the model simulations is similar to that for a constant relative humidity (γ^*).

Accompanying the stronger link between the variations of water vapor and temperature in the GCM simulations is a stronger coupling between the variation of water vapor in the interior of troposphere and those at the surface. In contrast, the phase relationships between variations of water vapor in the regions of ascending branches of the Hadley and Walker circulations and those in the regions of descending branches of the Hadley and Walker circulations appear to be well simulated by the GCM. It is suggested that the difference between the water vapor–temperature relationship in the model and that in the real atmosphere may be due to a stronger vertical mixing in the model atmosphere. One can imagine that convective adjustment, by saturating the adjusted column and ignoring mesoscale circulations, exaggerates the coupling between midtropospheric and near-surface water vapor. It will be of interest to compare these results with those from models with other convection schemes. Considering that numerical diffusion may also be a significant source of error, it will also be of interest to check whether these results change
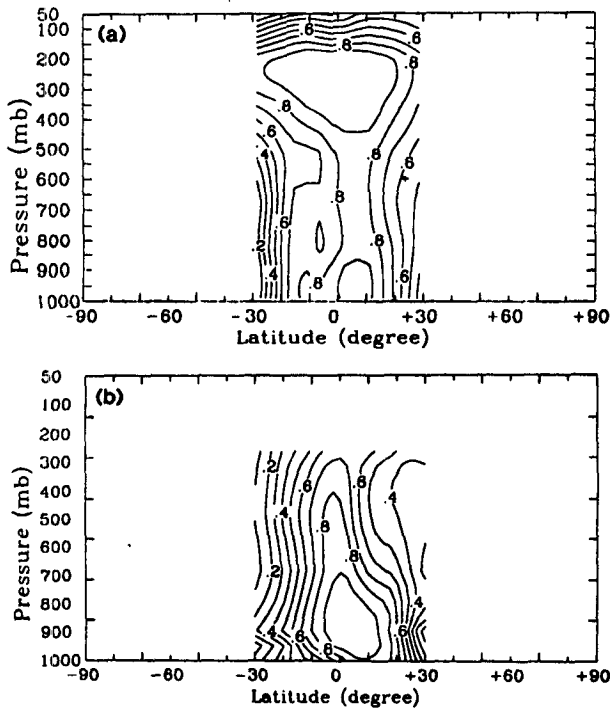
FIG. 14. The first EOF of the normalized zonal mean variations of q_a. The EOF is normalized so that its maximum value is 1: (a) model simulations; (b) observations.

FIG. 16. Vertical structure of the rate of fractional increase of tropical mean water vapor with temperature for the R15 model (solid line) and the R30 (dashed line).

results with those from models that have a better simulation of the tropical trade wind inversion.

The relevance of these results to the strength of water vapor feedback in global warming depends on the

when higher vertical resolution and different advection algorithms are used in the simulations. Since the largest discrepancies between the simulated and observed water vapor–temperature relationship are found in the region immediately above the tropical convective boundary layer, it is of particular interest to compare these
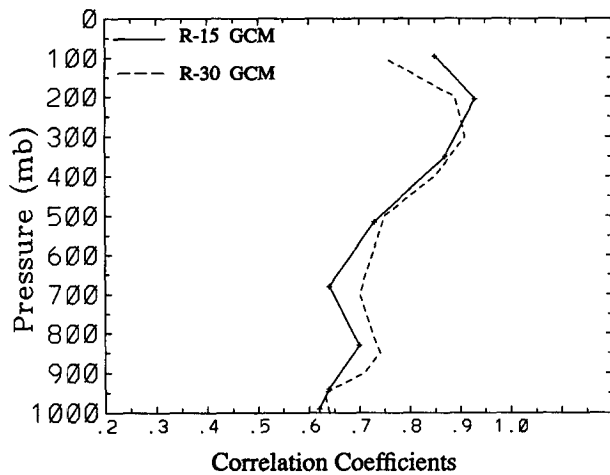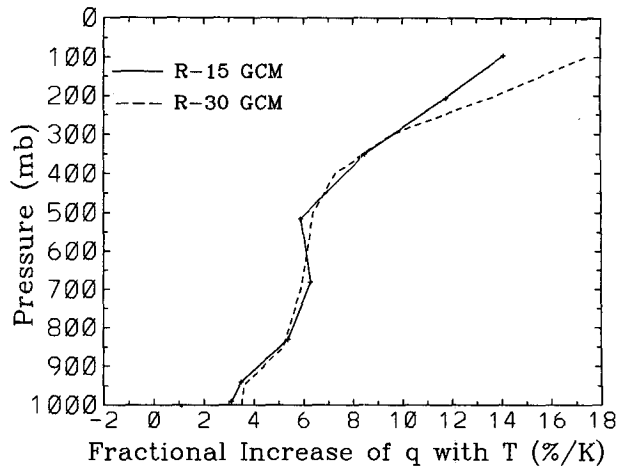

FIG. 15. Vertical structure of correlations between variations of $\langle T_a \rangle$ and $\langle q_a \rangle$ in the R15 GCM (solid line) and the R30 GCM (dashed line).
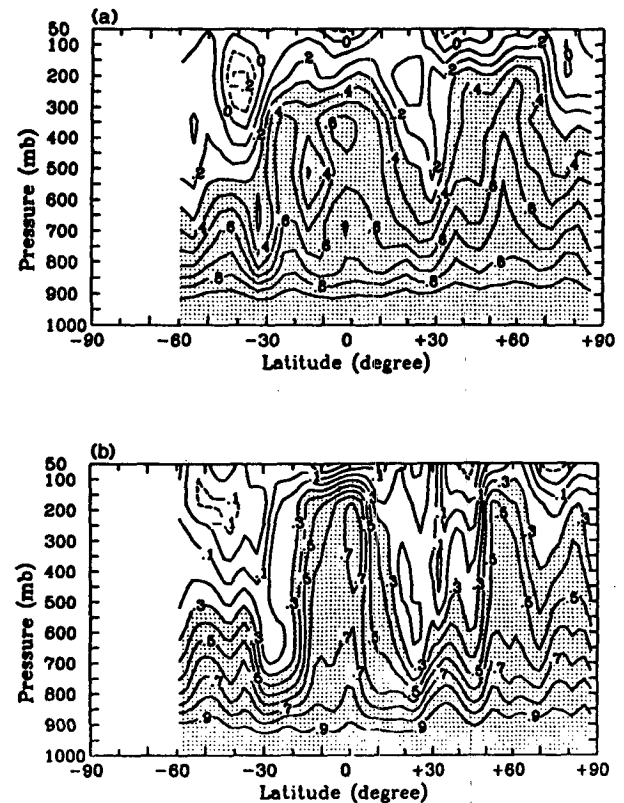

FIG. 17. Cross section of the correlations between variations of zonal mean specific humidity and those at the surface. Upper: R15 GCM; lower: R30 GCM.

premise that the tropical mean water vapor $\langle q \rangle$ is mainly controlled by tropical mean temperature $\langle T \rangle$. Accepting this premise, and using a one-dimensional model, it is estimated that over the tropical region (in a cloud-free atmosphere), the radiative feedback of water vapor in the GCM is stronger than that which exists in the observed atmosphere by about 30%. Since the Tropics are half the globe, this translates into a 15% enhancement of the globally averaged water vapor feedback. This premise, however, can be questioned. For example, one cannot rule out the possibility that $\langle q \rangle$ can change due to a redistribution of convection in the Tropics, without changing the mean convective heating or $\langle T \rangle$. In ENSO situations, the redistribution is concurrent with the change in $\langle T \rangle$, so we cannot conclude that the water vapor–temperature relationship on the interannual timescale will also hold for greenhouse warming. It would be desirable to design GCM experiments with SST anomalies to see if $\langle q \rangle$ can be altered without changing $\langle T \rangle$. Yet, it is impressive how closely $\langle q \rangle$ and $\langle T \rangle$ are correlated in the GCMs described here. It will be of interest to see if other GCMs, which predict a smaller $\gamma = \partial \langle q \rangle / \partial \langle T \rangle$ for interannual variations, also predict a smaller γ in global warming simulations.

It is also worth further exploring problems in the radiosonde data, in particular, the adequacy of the objective analysis scheme that has been used to interpolate station data onto a regular grid. It has been suggested that the objective analysis scheme may underestimate the interannual anomalies of water vapor over the eastern Pacific Ocean where stations are sparse (Sun and Oort 1995). An underestimate of the positive anomalies of water vapor over the eastern Pacific Ocean during an El Niño period will lead to a smaller $\langle q_a \rangle$ and a smaller γ. Though the agreement between the γ from the observations and the GCM simulations at the surface level suggests that the underestimate is not serious, it is worthwhile to quantify this underestimate and its impact on the calculation of γ in future research.

REFERENCES

Cess, R. D., and Coauthors, 1990: Intercomparison and interpretation of climate feedback processes in 19 atmospheric general circulation models. *J. Geophys. Res.,* **95,** 16 601–16 615.

Chou, M. D., 1986: Atmospheric solar heating rate in water vapor bands. *J. Climate Appl. Meteor.,* **25,** 1532–1542.

——, D. P. Krats, and W. Ridgway, 1991: Infrared radiation parameterizations in numerical climate models. *J. Climate,* **4,** 424–437.

Elliot, W. P., and D. J. Gaffen, 1991: On the utility of radiosonde archives for climate studies. *Bull. Amer. Meteor. Soc.,* **72,** 1507–1520.

Gaffen, D. J., T. P. Barnett, and W. P. Elliott, 1991: Space and time scales of global tropospheric moisture. *J. Climate,* **6,** 989–1008.

IPCC, 1992: *Climate Change: The Supplementary Report to The IPCC Scientific Assessment.* J. T. Houghton, B. A. Callander, and S. K. Varney, Eds., Intergovernmental Panel on Climate Change, Cambridge University Press, 364 pp.

Lau, N.-C., and M. J. Nath, 1994: A modeling study of the relative roles of tropical and extratropical SST anomalies in the variability of the global atmosphere–ocean system. *J. Climate,* **7,** 1184–1207.

Lindzen, R. S., 1990: Some coolness concerning global warming. *Bull. Amer. Meteor. Soc.,* **71,** 1465–1467.

Manabe, S., and R. T. Wetherald, 1967: Thermal equilibrium of the atmosphere with a given distribution of relative humidity. *J. Atmos. Sci.,* **50,** 241–259.

——, J. Smagrinsky, and R. F. Strickler, 1965: Simulated climatology of a general circulation model with a hydrological cycle. *Mon. Wea. Rev.,* **93,** 769–798.

McClatchey, R. A., R. W. Fenn, J. E. Selby, F. E. Volz, and J. S. Garing, 1972: *Optical Properties of the Atmosphere.* 3d ed., 108 pp.

Oort, A. H., 1983: Global Atmospheric Circulation Statistics, 1958–1973. NOAA Professional Paper 14, NOAA, U.S. Dept. of Commerce, Rockville, MD, 180 pp.

Peixoto, J. P., and A. H. Oort, 1992: *Physics of Climate.* American Institute of Physics, 520 pp.

Shine, K. P., and A. Sinha, 1991: Sensitivity of the earth's climate to height dependent changes in the water vapor mixing ratio. *Nature,* **354,** 382–384.

Soden, B., and R. Fu, 1995: A satellite analysis of deep convection, upper tropospheric humidity and greenhouse effect. *J. Climate,* **8,** 2333–2351.

Sun, D. Z., and R. S. Lindzen, 1993a: Distribution of tropical tropospheric water vapor. *J. Atmos. Sci.,* **50,** 1644–1660.

——, and ——, 1993b: Water vapor feedback and the ice-age snowline record. *Ann. Geophys.,* **11,** 204–215.

——, and A. H. Oort, 1995: Humidity-temperature relationships in the tropical troposphere. *J. Climate,* **8,** 1974–1987.